Observation of Non-Hermitian Topology with Nonunitary Dynamics of Solid-State Spins

Wengang Zhang,[1] Xiaolong Ouyang,[1] Xianzhi Huang,[1] Xin Wang,[1] Huili Zhang,[1] Yefei Yu[1], Xiuying Chang,[1] Yanqing Liu,[1] Dong-Ling Deng[1,2,*] and L.-M. Duan[1,†]

[1]*Center for Quantum Information, IIIS, Tsinghua University, Beijing 100084, People's Republic of China*
[2]*Shanghai Qi Zhi Institute, 41st Floor, AI Tower, No. 701 Yunjin Road, Xuhui District, Shanghai 200232, China*

Non-Hermitian topological phases exhibit a number of exotic features that have no Hermitian counterparts, including the skin effect and breakdown of the conventional bulk-boundary correspondence. Here, we implement the non-Hermitian Su-Schrieffer-Heeger Hamiltonian, which is a prototypical model for studying non-Hermitian topological phases, with a solid-state quantum simulator consisting of an electron spin and a ^{13}C nuclear spin in a nitrogen-vacancy center in a diamond. By employing a dilation method, we realize the desired nonunitary dynamics for the electron spin and map out its spin texture in the momentum space, from which the corresponding topological invariant can be obtained directly. From the measured spin textures with varying parameters, we observe both integer and fractional winding numbers. The non-Hermitian topological phase with fractional winding number cannot be continuously deformed to any Hermitian topological phase and is intrinsic to non-Hermitian systems. Our result paves the way for further exploiting and understanding the intriguing properties of non-Hermitian topological phases with solid-state spins or other quantum simulation platforms.

While Hermiticity lies at the heart of quantum mechanics, non-Hermitian Hamiltonians have widespread applications as well [1–3]. Indeed, they have been extensively studied in photonic systems with loss and gain [4–9], open quantum systems [10–15], and quasiparticles with finite lifetimes [16–18], etc. Recently, the interplay between non-Hermiticity and topology has attracted tremendous attention [19,20], giving rise to an emergent research frontier of non-Hermitian topological phases of matter. In contrast to topological phases for Hermitian systems [21–23], non-Hermitian ones bears several peculiar features, such as the skin effect [24–26] and breakdown of the conventional bulk-boundary correspondence [25–30], and new topological classifications [31–33]. In particular, the non-Hermitian skin effect describes an exotic phenomena that possesses no counterpart in Hermitian systems, where the majority of the eigenstates of a non-Hermitian Hamiltonian are exponentially localized at boundaries. This localization of the bulk states leads to the breakdown of the conventional bulk-boundary correspondence and suggests a non-Bloch band theory in which a non-Bloch topological invariant could be defined to restore a generalized bulk-boundary correspondence beyond the conventional framework [25,26]. The non-Hermitian skin effect would also dramatically alter the long-time dynamics of an open quantum system, resulting in a chiral damping phenomena [34]. More recently, its unusual consequences have been investigated in the context of machine learning topological phases [35], where it is shown that this effect would cause a critical obstacle for the straightforward extension of the unsupervised method for learning Hermitian topological phases to the non-Hermitian scenario.

Experimental observations of the non-Hermitian skin effect have been reported in mechanical metamaterials [36], nonreciprocal topolectric circuits [37], and photonic systems [38,39]. However, despite the notable progress, direct observation of the topological invariant for non-Hermitian systems has not been reported in a quantum solid-state system hitherto, owing to the stringent requirement of delicate engineering of the coupling between the target system and the environment in implementing non-Hermitian Hamiltonians. In this Letter, we carry out such an experiment and report the direct observation of the non-Hermitian topological invariant with a solid-state quantum simulator consisting of both electron and nuclear spins in a nitrogen-vacancy (NV) center (see Fig. 1).

NV centers in diamonds [40] exhibit atomlike properties, such as long-lived spin quantum states and well-defined optical transitions, which make them an excellent experimental platform for quantum information processing [41–46], sensing [47–49], and quantum simulation [50–52]. For Hermitian topological phases, simulations of three-dimensional (3D) Hopf insulators [50] and chiral topological insulators [51] with NV centers have been demonstrated in recent experiments, and observations of their topological properties, such as nontrivial topological links associated with the Hopf fibration and the integer-valued topological invariants, have been reported. A key idea that enables these simulations is to use the adiabatic passage technique, where we treat the momentum-space Hamiltonian as a
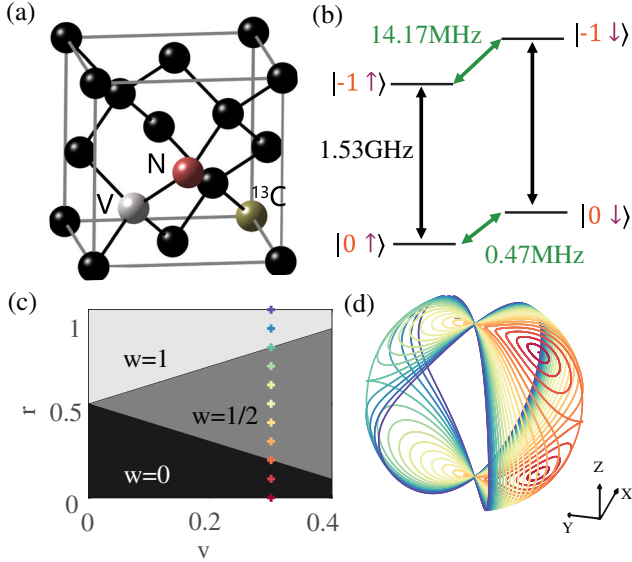
FIG. 1. Experimental system and topological properties of the non-Hermitian Su-Schrieffer-Heeger (SSH) model. (a) Illustration of the NV center platform used in this work. The electron spin is coupled to a nearby ^{13}C nuclear spin with 13.7 MHz hyperfine interaction. (b) Energy level structure of the electron-nuclear spin system. Black arrows indicate the microwave transitions. Green arrows indicate the radio frequency transition. We choose $|0\rangle$ and $|-1\rangle$ to consist our electron-spin qubit. $|\uparrow\rangle$ and $|\downarrow\rangle$ denote the nuclear spin state. (c) A sketch of the phase diagram of the non-Hermitian SSH Hamiltonian $H(k)$. (d) Trajectories of the right eigenvectors of $H(k)$ on the Bloch sphere with varying parameters as k sweeps through the first Brillouin zone. Different trajectories correspond to the markers with the same color as shown in (c).

time-dependent one with the momentum playing the role of time. The ground state of the Hamiltonian at different momentum points can be obtained via adiabatically tuning the frequency and the amplitude of a microwave that manipulates the electron spin in the center, and quantum tomography of the final state with a varying momentum provides all the information needed for obtaining the characteristic topological properties [50].

Nevertheless, simulating non-Hermitian topological phases with the NV center platform [see Figs. 1(a) and 1(b)] faces two apparent challenges. First, for non-Hermitian systems the governing Hamiltonians typically have complex eigenenergies and the conventional adiabatic theorem is not necessarily valid in general [53]. As a consequence, the adiabatic passage technique may not apply and the preparation of eigenstates of non-Hermitian Hamiltonians becomes trickier. Second, the non-Hermiticity requires a delicate engineering of the coupling between the targeted system and the environment, so that tracing out the environment could leave the system effectively governed by a given non-Hermitian Hamiltonian. These two challenges make simulating non-Hermitian topological phases notably more difficult than that for their Hermitian counterparts.

In this Letter, we overcome these two challenges and report the first experimental demonstration of simulating non-Hermitian topological phases with the NV center platform. In particular, we implement a prototypical model for studying non-Hermitian topological phases, i.e., the non-Hermitian Su-Schrieffer-Heeger (SSH) model, by carefully engineering the coupling between the electron and nuclear spins through a dilation method [54–57]. Without using adiabatic passage, we find that the nonunitary dynamics generated by the non-Hermitian Hamiltonian will autonomously drive the electron spin into the eigenstate of the Hamiltonian with the largest imaginary eigenvalue, independent of its initial state. The topological nature of the Hamiltonian can be visualized by mapping out the spin texture in the momentum space and the topological invariant can be derived directly by a discretized integration over the momentum space. From the measured spin textures at different model parameters, we observe both integer and fractional winding numbers. Whereas the topological phases with integer winding numbers might be continuously deformed to the Hermitian ones, the observed fractional winding number captures intrinsic non-Hermitian topology and possesses no counterpart in Hermitian systems.

To start with, we consider the following non-Hermitian SSH model Hamiltonian in the momentum space [26,27,58,59]:

$$H(k) = \gamma\left[h_x\sigma_x + \left(h_z + \frac{i}{2}\right)\sigma_z\right], \qquad (1)$$

where γ measures the energy scale (we set $\hbar = 1$ for simplicity), $h_x = v + r\cos k$, $h_z = r\sin k$, and $\sigma_{x,z}$ are the usual Pauli matrices. This Hamiltonian possesses a sublattice symmetry $\sigma_y^{-1}H(k)\sigma_y = -H(k)$, which ensures that its eigenvalues appear in $(E, -E)$ pairs. Its energy gap closes at the exceptional points $(h_x, h_z) = (\pm\frac{1}{2}, 0)$, which gives $v = r \pm \frac{1}{2}$ for $k = \pi$ and $v = -r \pm \frac{1}{2}$ for $k = 0$. The topological properties for the Hamiltonian can be characterized by the winding number w of $H(k)$, circling around the exceptional points as k sweeps through the first Brillouin zone [27,60]: $w = 0$, $\frac{1}{2}$, and 1 respectively, if $H(k)$ encircles zero, one, and two exceptional points. A direct calculation yields $w = 0$ for $|v \pm \frac{1}{2}| > |r|$, $w = \frac{1}{2}$ for $|v \pm \frac{1}{2}| < |r|$ and $|r| < \frac{1}{2}$, and $w = 1$ for $|v \pm \frac{1}{2}| < |r|$ and $|r| > \frac{1}{2}$. A sketch of the phase diagram of the non-Hermitian SSH model is shown in Fig. 1(c) and the trajectories of the right eigenstates of $H(k)$ as k sweeps the first Brillouin zone is plotted Fig. 1(d).

Studying non-Hermitian quantum physics in experiment is challenging, since closed quantum systems are governed by Hermitian Hamiltonians. To this end, theoretical approaches have been introduced to dilate parity-time symmetric Hamiltonians into Hermitian ones in a larger

Hilbert space [54,55]. More recently, the dilation method has been used in experiments to realize nonunitary quantum dynamics for photons [56] and to implement arbitrary single-qubit non-Hermitian Hamiltonians and study parity-time symmetry breaking with NV centers [57]. To implement $H(k)$ in our experiment, we exploit the dilation method and use the electron spin as the targeted system and a nearby ^{13}C nuclear spin as the ancillary qubit. Suppose that the dynamics of the electron spin is described by H_e and the dilated system described by $H_{e,n}$, then the problem essentially reduces to a task that for a given momentum k we need to carefully engineer $H_{e,n}$, such that H_e equals $H(k)$ after projecting the nuclear spin onto a desired state. The basic idea is as follows. We consider a quantum state $|\psi\rangle$ evolving under a non-Hermitian Hamiltonian H_e, which satisfies the Schrödinger equation $i(\partial/\partial t)|\psi(t)\rangle = H_e|\psi(t)\rangle$. Then we introduce a dilated state $|\Psi(t)\rangle = |\psi(t)\rangle|-\rangle + \eta(t)|\psi(t)\rangle|+\rangle$ governed by the dilated Hermitian Hamiltonian $H_{e,n}$. Here, $|-\rangle = (|\uparrow\rangle - i|\downarrow\rangle)/\sqrt{2}$, $|+\rangle = -i(|\uparrow\rangle + i|\downarrow\rangle)/\sqrt{2}$ and $\eta(t)$ is a proper time-dependent linear operator. The dilated system satisfies $i(\partial/\partial t)|\Psi(t)\rangle = H_{e,n}|\Psi(t)\rangle$. For our purpose, the dilated Hamiltonian should be designed properly as [61]

$$H_{e,n} = [A_0(t)\mathbf{I} + A_1(t)\sigma_x + A_2(t)\sigma_y + A_3(t)\sigma_z] \otimes \mathbf{I}$$
$$+ [B_0(t)\mathbf{I} + B_1(t)\sigma_x + B_2(t)\sigma_y + B_3(t)\sigma_z] \otimes \sigma_z,$$
$$(2)$$

where $\mathbf{I}$ is the two-by-two identity matrix, and $A_i(t)$ and $B_i(t)$ ($i = 0, 1, 2, 3$) are time-dependent real-valued functions determined by H_e. The dilated Hamiltonian $H_{e,n}$ is Hermitian and $|\Psi(t)\rangle$ undergoes a unitary evolution. Through measuring the state $|\Psi(t)\rangle$, the nonunitary evolution of $|\psi(t)\rangle$ under H_e can be obtained in the $|-\rangle\langle-|$ subspace of the nuclear spin [61].

Unlike the case of simulating Hermitian topological phases [50,51], where the ground state of the Hamiltonian at different momentum points can be obtained through adiabatic passages, for non-Hermitian Hamiltonians their eigenvalues are complex numbers in general and the adiabatic passage method does not apply directly. Fortunately, we can explore the nonunitary dynamics generated by the non-Hermitian Hamiltonian to prepare the eigenstate that corresponds to the eigenvalue with the largest imaginary part. To be more specific, suppose the electron spin is initially at an arbitrary state $|\psi(0)\rangle = \alpha_1|R_1\rangle + \alpha_2|R_2\rangle$, where $|R_{1,2}\rangle$ are the right eigenstates of H_e corresponding to the eigenvalues $\lambda_{1,2}$. Without loss of generality, we assume $\text{Im}(\lambda_1) > \text{Im}(\lambda_2)$. Then the electron spin state will decay to $|R_1\rangle$ in the long time limit. As a result, we can prepare the eigenstate $|R_1\rangle$ of H_e by just waiting long enough time for the system to decay to this state.
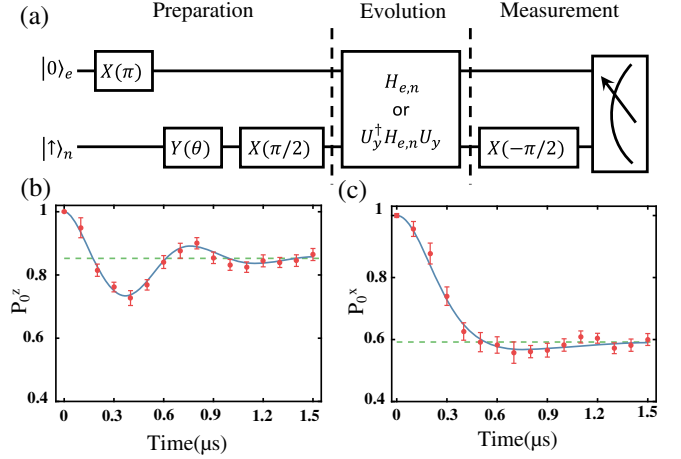

FIG. 2. (a) The quantum circuits used in our experiment. Through optical pumping, we first polarize the electron and nuclear spins onto $|0\rangle_e$ and $|\uparrow\rangle_n$, respectively [62–65]. Then, rotations along x and y axes will prepare the dilated system onto the state $|\Psi(0)\rangle = |-1\rangle_e|-\rangle_n + \eta(0)|-1\rangle_e|+\rangle_n$. The evolution box implements the unitary dynamics generated by the dilated Hamiltonian $H_{e,n}$, after which we measure the nuclear spin in the $|\pm\rangle$ basis [66–68]. A postselection of nuclear spin in the $|-\rangle$ state collapses the electron spin into the desired eigenstate of $H_e = H(k)$ for a given momentum k. (b), (c) Benchmark of the nonunitary time evolution. Here, we plot the time evolution (under the Hamiltonian H_e) of the populations $P_0^z = \text{Tr}(\rho_e|0\rangle_e\langle0|)$ and $P_0^x = \text{Tr}(\rho_e|+\rangle_e\langle+|)$ with $|+\rangle_e = (1/\sqrt{2})(|0\rangle + |-1\rangle)$. For (b) and (c), the parameters characterizing the underlying Hamiltonian are chosen as $v = 0.3$, $r = 1$, $\gamma = 3.5$, and $k = 0.3\pi$, and $v = 0.3$, $r = 0.3$, $\gamma = 4$, and $k = 0.6\pi$, respectively. Here, the solid lines plot the theoretical predictions and the dashed green lines indicate the theoretical population of the targeted state at the long time limit [61].

To experimentally realize $H_{e,n}$, we apply two microwave pulses with time-dependent amplitude, frequency, and phase. We explore the state evolution by monitoring the population on $|0\rangle_e$ state and see how it decays to the desired eigenstate of H_e. In Fig. 2(a), we show the quantum circuits used in our experiment. Figures 2(b) and 2(c) show our experimental results of $P_0^{z,x}$ as a function of time. From these figures, it is evident that our experimental results match the theoretical predictions excellently, within the error bars for almost all of the data points. In addition, after long enough evolution time (about 1.5 μs in our experiment), the electron spin state decays to the desired eigenstate of $H(k)$ for different momentum k. This indicates that our dilated Hamiltonian indeed effectively implements the non-Hermitian $H(k)$ in our experiment.

We mention that in Fig. 2(c), we measure P_0 in the x basis, which requires a $\pi/2$ rotation of the electron spin. In order to avoid off-resonance driving, the microwave driving power should be weak enough. The Rabi frequency should be much smaller than the hyperfine coupling strength (13.7 MHz), so that the $\pi/2$ rotation would take time on
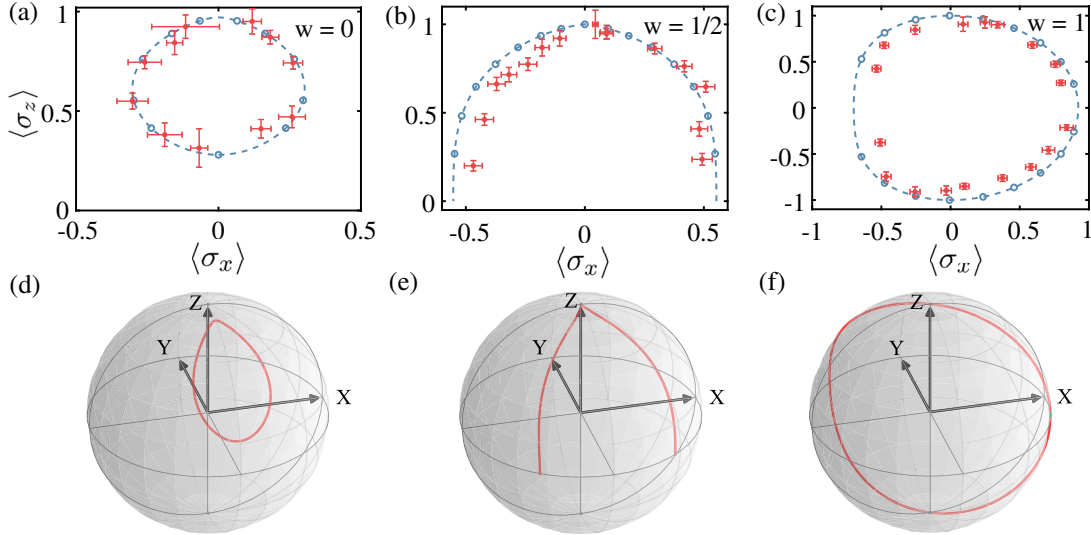
FIG. 3. The trajectory of the target eigenvector of $H(k)$ in the Brillouin zone. (a), (b), and (c) plot the experimental results of $\langle\sigma_z\rangle$ versus $\langle\sigma_x\rangle$ as k sweeps the first Brillouin zone. Here, the red dots with error bars denote the experimental data, whereas the blue dots with dashed curves represent the theoretical prediction from numerical simulations. The parameters are chosen as $v = 0.3$ and $r = 0.18$, 0.3, 1 in (a), (b), and (c) respectively, with corresponding winding number $w = 0, \frac{1}{2}, 1$. (d), (e), and (f) show the theoretical trajectories of the electron spin state on the Bloch sphere, whose projections onto the xz plane correspond to (a), (b), and (c), respectively.

the order of a microsecond. Meanwhile, the time evolution process also takes approximately half of the system's coherence time ($T_2^\star = 3.3~\mu$s). Thus, adding an additional rotation would not only increase the processing time but also introduce both gate and decoherence errors. To avoid this, we first apply a unitary transform to the target Hamiltonian: $\widetilde{H}_e = U_y^\dagger H_e U_y$, where $U_y = (1/\sqrt{2})\bigl(\begin{smallmatrix}1 & -1\\ 1 & 1\end{smallmatrix}\bigr)$. We evolve the electron spin with $\widetilde{H}_e$ instead of H_e and measure the final state in the z basis. This is equivalent to evolving the electron spin with H_e and then measuring in the x basis, but with improved efficiency and accuracy [61]. In addition, the time needed for the initial state to decay to the desired eigenstate of H_e depends crucially on the difference between the imaginary parts of its two eigenvalues. For some parameter regions, this difference may not be large enough and the decay time could even be longer than $T_2^\star$. To speedup the process, we increase γ according to the specific parameters so that we can finish the experiment within the coherence time.

To probe the topological properties of the non-Hermitian SSH model, we can measure $\langle\sigma_z\rangle$ and $\langle\sigma_x\rangle$ for the final state of the time evolution as k sweeps the Brillouin zone. We plot our experimental results in Fig. 3. When $H(k)$ encircles no or two exceptional points, the eigenvectors of $H(k)$ are 2π periodic in k, and the trajectory of $\langle\sigma_z\rangle$ and $\langle\sigma_x\rangle$ as k sweeps through the Brillouin zone forms closed circles. In this case, the winding number is zero or one, depending on whether the trajectory of $\langle\sigma_z\rangle$ and $\langle\sigma_x\rangle$ winds around the origin or not, as clearly shown in Figs. 3(a) and 3(c). In contrast, when $H(k)$ encircles only one exceptional point, the eigenvector will have a 4π periodicity and k must

sweep through 4π to close the trajectory, giving rise to a fractional value of the winding number $w = \frac{1}{2}$ if k only sweeps through the first Brillouin zone [27]. This is also explicitly observed in our experiment as shown in Fig. 3(b). We mention that in Fig. 3(c), when k sweeps across π, the imaginary part of the eigenvalues of $H(k)$ will exchange their sign, leading to a leap from one eigenstate to another. Mathematically, we can prove that $\langle R_1|\sigma_{z,x}|R_1\rangle = -\langle R_2|\sigma_{z,x}|R_2\rangle$ and $\langle R_1|\sigma_y|R_1\rangle = \langle R_2|\sigma_y|R_2\rangle$ [61]. As a result, in the experiment we obtain $\langle R_1|\sigma_{z,x}|R_1\rangle$ by actually measuring $\langle R_2|\sigma_{z,x}|R_2\rangle$ after the crossing of the eigenstates. In addition, with our experimentally measured data the winding number can also be calculated directly through a discretized integration over the momentum space [61]. In Table I, we show the winding number calculated from the experimental and theoretically simulated data for different parameter values of r [69]. From this table, it is clear that the winding number calculated from the experimental data matches its theoretical predictions within a good precision, and is in agreement with that obtained from the trajectory of $\langle\sigma_z\rangle$ and $\langle\sigma_x\rangle$.

We stress that the observation of the fractional winding number in our experiment is crucial because it captures a signature of intrinsic non-Hermitian topology. For the integer winding number, it corresponds to the line-gap topology and the corresponding topological phases are continuously deformable to the Hermitian ones. Whereas, the fractional winding number corresponds to point-gap topology and is intrinsic to non-Hermitian systems with *no* counterparts in Hermitian systems [33,70]. In our

TABLE I. The winding number extracted from the experimental and numerically simulated data. Here, the model parameters are chosen the same as in Fig. 3. For $r = 0.3$, $H(k)$ only encircles one exceptional point and its eigenvector has a 4π periodicity. As a result, for this case we sweep the momentum k through $[0, 4\pi]$ to form a closed loop so that the discretized integration for computing the winding number is well-defined [61].

Winding number w	Experiment	Theory
$r = 0.18(k : 0 \rightarrow 2\pi)$	0.0004 ± 0.0273	0.0000
$r = 0.30(k : 0 \rightarrow 4\pi)$	0.9954 ± 0.0154	1.0000
$r = 1.00(k : 0 \rightarrow 2\pi)$	1.0084 ± 0.0144	1.0000

experiment, we observe both integer and fractional winding numbers, which unambiguously confirms the exotic and intrinsic non-Hermitian topology carried by the simple but illuminating non-Hermitian SSH model. We also note that, under the open boundary condition, the non-Hermitian SSH model will exhibit the non-Hermitian skin effect due to the correspondence between intrinsic non-Hermitian topology and the skin effect [30,70,71]. In the future, it would be interesting and important to observe the skin effect in a quantum solid-state system. Our current experiment uses only two spins of an NV center and treats the momentum k as a parameter of the SSH Hamiltonian. As a result, it is not capable of implementing this non-Hermitian Hamiltonian in real space so as to observe the desired skin effect. Accomplishing this requires delicate and accurate engineering of interactions between many spins, which is still challenging with the state-of-the-art NV technologies.

In summary, we have experimentally observed the non-Hermitian topological properties of the SSH model through nonunitary dynamics with a solid state quantum simulator. Our method carries over straightforwardly to other types of non-Hermitian topological models that are predicted to exist in the extended periodic table [31–33] but have not yet been observed in any experiment. It thus paves the way for future explorations of exotic non-Hermitian topological phases with the NV center or other quantum simulation platforms.

[*]dldeng@tsinghua.edu.cn
[†]lmduan@tsinghua.edu.cn

[1] N. Moiseyev, *Non-Hermitian Quantum Mechanics* (Cambridge University Press, Cambridge, England, 2011).

[2] V. V. Konotop, J. Yang, and D. A. Zezyulin, Nonlinear waves in $\mathcal{PT}$-symmetric systems, Rev. Mod. Phys. **88**, 035002 (2016).

[3] Y. Ashida, Z. Gong, and M. Ueda, Non-Hermitian physics, Adv. Phys. **69**, 249 (2020).

[4] L. Feng, Y.-L. Xu, W. S. Fegadolli, M.-H. Lu, J. E. Oliveira, V. R. Almeida, Y.-F. Chen, and A. Scherer, Experimental demonstration of a unidirectional reflectionless parity-time metamaterial at optical frequencies, Nat. Mater. **12**, 108 (2013).

[5] B. Peng, Ş. Özdemir, S. Rotter, H. Yilmaz, M. Liertzer, F. Monifi, C. Bender, F. Nori, and L. Yang, Loss-induced suppression and revival of lasing, Science **346**, 328 (2014).

[6] L. Xiao, X. Zhan, Z. Bian, K. Wang, X. Zhang, X. Wang, J. Li, K. Mochizuki, D. Kim, N. Kawakami et al., Observation of topological edge states in parity–time-symmetric quantum walks, Nat. Phys. **13**, 1117 (2017).

[7] R. El-Ganainy, K. G. Makris, M. Khajavikhan, Z. H. Musslimani, S. Rotter, and D. N. Christodoulides, Non-Hermitian physics and pt symmetry, Nat. Phys. **14**, 11 (2018).

[8] L. Feng, R. El-Ganainy, and L. Ge, Non-Hermitian photonics based on parity–time symmetry, Nat. Photonics **11**, 752 (2017).

[9] T. Ozawa, H. M. Price, A. Amo, N. Goldman, M. Hafezi, L. Lu, M. C. Rechtsman, D. Schuster, J. Simon, O. Zilberberg, and I. Carusotto, Topological photonics, Rev. Mod. Phys. **91**, 015006 (2019).

[10] J. Dalibard, Y. Castin, and K. Mølmer, Wave-Function Approach to Dissipative Processes in Quantum Optics, Phys. Rev. Lett. **68**, 580 (1992).

[11] J. Anglin, Cold, Dilute, Trapped Bosons as an Open Quantum System, Phys. Rev. Lett. **79**, 6 (1997).

[12] I. Rotter, A non-hermitian hamilton operator and the physics of open quantum systems, J. Phys. A **42**, 153001 (2009).

[13] B. Zhen, C. W. Hsu, Y. Igarashi, L. Lu, I. Kaminer, A. Pick, S.-L. Chua, J. D. Joannopoulos, and M. Soljačić, Spawning rings of exceptional points out of Dirac cones, Nature (London) **525**, 354 (2015).

[14] S. Diehl, E. Rico, M. A. Baranov, and P. Zoller, Topology by dissipation in atomic quantum wires, Nat. Phys. **7**, 971 (2011).

[15] F. Verstraete, M. M. Wolf, and J. I. Cirac, Quantum computation and quantum-state engineering driven by dissipation, Nat. Phys. **5**, 633 (2009).

[16] H. Shen and L. Fu, Quantum Oscillation from In-Gap States and a Non-Hermitian Landau Level Problem, Phys. Rev. Lett. **121**, 026403 (2018).

[17] H. Zhou, C. Peng, Y. Yoon, C. W. Hsu, K. A. Nelson, L. Fu, J. D. Joannopoulos, M. Soljačić, and B. Zhen, Observation of bulk Fermi arc and polarization half charge from paired exceptional points, Science **359**, 1009 (2018).

[18] T. Yoshida, R. Peters, and N. Kawakami, Non-Hermitian perspective of the band structure in heavy-fermion systems, Phys. Rev. B **98**, 035141 (2018).

[19] E. J. Bergholtz, J. C. Budich, and F. K. Kunst, Exceptional topology of non-Hermitian systems, Rev. Mod. Phys. **93**, 015005 (2021).

[20] C. Coulais, R. Fleury, and J. van Wezel, Topology and broken hermiticity, Nat. Phys., **17**, 9 (2021).

[21] X.-L. Qi and S.-C. Zhang, Topological insulators and superconductors, Rev. Mod. Phys. **83**, 1057 (2011).

[22] M. Z. Hasan and C. L. Kane, Colloquium: Topological insulators, Rev. Mod. Phys. **82**, 3045 (2010).

[23] C.-K. Chiu, J. C. Y. Teo, A. P. Schnyder, and S. Ryu, Classification of topological quantum matter with symmetries, Rev. Mod. Phys. **88**, 035005 (2016).

[24] A. McDonald, T. Pereg-Barnea, and A. A. Clerk, Phase-Dependent Chiral Transport and Effective Non-Hermitian Dynamics in a Bosonic Kitaev-Majorana Chain, Phys. Rev. X **8**, 041031 (2018).

[25] F. K. Kunst, E. Edvardsson, J. C. Budich, and E. J. Bergholtz, Biorthogonal Bulk-Boundary Correspondence in Non-Hermitian Systems, Phys. Rev. Lett. **121**, 026808 (2018).

[26] S. Yao and Z. Wang, Edge States and Topological Invariants of Non-Hermitian Systems, Phys. Rev. Lett. **121**, 086803 (2018).

[27] T. E. Lee, Anomalous Edge State in a Non-Hermitian Lattice, Phys. Rev. Lett. **116**, 133903 (2016).

[28] K. Yokomizo and S. Murakami, Non-Bloch Band Theory of Non-Hermitian Systems, Phys. Rev. Lett. **123**, 066404 (2019).

[29] V. M. Alvarez, J. B. Vargas, M. Berdakin, and L. F. Torres, Topological states of non-Hermitian systems, Eur. Phys. J. Spec. Top. **227**, 1295 (2018).

[30] D. S. Borgnia, A. J. Kruchkov, and R.-J. Slager, Non-Hermitian Boundary Modes and Topology, Phys. Rev. Lett. **124**, 056802 (2020).

[31] K. Kawabata, K. Shiozaki, M. Ueda, and M. Sato, Symmetry and Topology in Non-Hermitian Physics, Phys. Rev. X **9**, 041015 (2019).

[32] H. Zhou and J. Y. Lee, Periodic table for topological bands with non-Hermitian symmetries, Phys. Rev. B **99**, 235112 (2019).

[33] K. Kawabata, S. Higashikawa, Z. Gong, Y. Ashida, and M. Ueda, Topological unification of time-reversal and particle-hole symmetries in non-Hermitian physics, Nat. Commun. **10**, 297 (2019).

[34] F. Song, S. Yao, and Z. Wang, Non-Hermitian Skin Effect and Chiral Damping in Open Quantum Systems, Phys. Rev. Lett. **123**, 170401 (2019).

[35] L.-W. Yu and D.-L. Deng, Unsupervised Learning of Non-Hermitian Topological Phases, Phys. Rev. Lett. **126**, 240402 (2021).

[36] A. Ghatak, M. Brandenbourger, J. van Wezel, and C. Coulais, Observation of non-Hermitian topology and its bulk–edge correspondence in an active mechanical metamaterial, Proc. Natl. Acad. Sci. U.S.A. **117**, 29561 (2020).

[37] T. Helbig, T. Hofmann, S. Imhof, M. Abdelghany, T. Kiessling, L. Molenkamp, C. Lee, A. Szameit, M. Greiter, and R. Thomale, Generalized bulk–boundary correspondence in non-Hermitian topolectrical circuits, Nat. Phys. **16**, 747 (2020).

[38] L. Xiao, T. Deng, K. Wang, G. Zhu, Z. Wang, W. Yi, and P. Xue, Non-Hermitian bulk–boundary correspondence in quantum dynamics, Nat. Phys. **16**, 761 (2020).

[39] S. Weidemann, M. Kremer, T. Helbig, T. Hofmann, A. Stegmaier, M. Greiter, R. Thomale, and A. Szameit, Topological funneling of light, Science **368**, 311 (2020).

[40] M. W. Doherty, N. B. Manson, P. Delaney, F. Jelezko, J. Wrachtrup, and L. C. Hollenberg, The nitrogen-vacancy colour centre in diamond, Phys. Rep. **528**, 1 (2013).

[41] J. Wrachtrup, S. Y. Kilin, and A. Nizovtsev, Quantum computation using the 13 c nuclear spins near the single nv defect center in diamond, Opt. Spectrosc. **91**, 429 (2001).

[42] Y. Wu, Y. Wang, X. Qin, X. Rong, and J. Du, A programmable two-qubit solid-state quantum processor under ambient conditions, npj Quantum Inf. **5**, 9 (2019).

[43] H. Bernien, B. Hensen, W. Pfaff, G. Koolstra, M. S. Blok, L. Robledo, T. Taminiau, M. Markham, D. J. Twitchen, L. Childress *et al.*, Heralded entanglement between solid-state qubits separated by three metres, Nature (London) **497**, 86 (2013).

[44] P. C. Humphreys, N. Kalb, J. P. Morits, R. N. Schouten, R. F. Vermeulen, D. J. Twitchen, M. Markham, and R. Hanson, Deterministic delivery of remote entanglement on a quantum network, Nature (London) **558**, 268 (2018).

[45] S. Schmitt, T. Gefen, F. M. Stürner, T. Unden, G. Wolff, C. Müller, J. Scheuer, B. Naydenov, M. Markham, S. Pezzagna *et al.*, Submillihertz magnetic spectroscopy performed with a nanoscale quantum sensor, Science **356**, 832 (2017).

[46] J.-W. Zhou, P.-F. Wang, F.-Z. Shi, P. Huang, X. Kong, X.-K. Xu, Q. Zhang, Z.-X. Wang, X. Rong, and J.-F. Du, Quantum information processing and metrology with color centers in diamonds, Front. Phys. **9**, 587 (2014).

[47] G. Balasubramanian, I. Chan, R. Kolesov, M. Al-Hmoud, J. Tisler, C. Shin, C. Kim, A. Wojcik, P. R. Hemmer, A. Krueger *et al.*, Nanoscale imaging magnetometry with diamond spins under ambient conditions, Nature (London) **455**, 648 (2008).

[48] S. Kolkowitz, A. Safira, A. High, R. Devlin, S. Choi, Q. Unterreithmeier, D. Patterson, A. Zibrov, V. Manucharyan, H. Park *et al.*, Probing Johnson noise and ballistic transport in normal metals with a single-spin qubit, Science **347**, 1129 (2015).

[49] G. Kucsko, P. C. Maurer, N. Y. Yao, M. Kubo, H. J. Noh, P. K. Lo, H. Park, and M. D. Lukin, Nanometre-scale thermometry in a living cell, Nature (London) **500**, 54 (2013).

[50] X.-X. Yuan, L. He, S.-T. Wang, D.-L. Deng, F. Wang, W.-Q. Lian, X. Wang, C.-H. Zhang, H.-L. Zhang, X.-Y. Chang *et al.*, Observation of topological links associated with Hopf insulators in a solid-state quantum simulator, Chin. Phys. Lett. **34**, 060302 (2017).

[51] W. Lian, S.-T. Wang, S. Lu, Y. Huang, F. Wang, X. Yuan, W. Zhang, X. Ouyang, X. Wang, X. Huang *et al.*, Machine Learning Topological Phases with a Solid-State Quantum Simulator, Phys. Rev. Lett. **122**, 210503 (2019).

[52] G. Kucsko, S. Choi, J. Choi, P. C. Maurer, H. Zhou, R. Landig, H. Sumiya, S. Onoda, J. Isoya, F. Jelezko *et al.*, Critical Thermalization of a Disordered Dipolar Spin System in Diamond, Phys. Rev. Lett. **121**, 023601 (2018).

[53] S. Ibáñez and J. G. Muga, Adiabaticity condition for non-Hermitian Hamiltonians, Phys. Rev. A **89**, 033403 (2014).

[54] U. Günther and B. F. Samsonov, Naimark-Dilated $\mathcal{PT}$-Symmetric Brachistochrone, Phys. Rev. Lett. **101**, 230404 (2008).

[55] K. Kawabata, Y. Ashida, and M. Ueda, Information Retrieval and Criticality in Parity-Time-Symmetric Systems, Phys. Rev. Lett. **119**, 190401 (2017).

[56] L. Xiao, K. Wang, X. Zhan, Z. Bian, K. Kawabata, M. Ueda, W. Yi, and P. Xue, Observation of Critical Phenomena in Parity-Time-Symmetric Quantum Dynamics, Phys. Rev. Lett. **123**, 230401 (2019).

[57] Y. Wu, W. Liu, J. Geng, X. Song, X. Ye, C.-K. Duan, X. Rong, and J. Du, Observation of parity-time symmetry breaking in a single-spin system, Science **364**, 878 (2019).

[58] X. Zhu, H. Wang, S. K. Gupta, H. Zhang, B. Xie, M. Lu, and Y. Chen, Photonic non-Hermitian skin effect and non-Bloch bulk-boundary correspondence, Phys. Rev. Research **2**, 013280 (2020).

[59] S. Lieu, Topological phases in the non-Hermitian Su-Schrieffer-Heeger model, Phys. Rev. B **97**, 045106 (2018).

[60] O. Viyuela, D. Vodola, G. Pupillo, and M. A. Martin-Delgado, Topological massive Dirac edge modes and long-range superconducting Hamiltonians, Phys. Rev. B **94**, 125121 (2016).

[61] See Supplemental Material at http://link.aps.org/supplemental/10.1103/PhysRevLett.127.090501 for details on the experimental setup, the diamond sample used, the initialization and readout of the spin states, the derivation of the dilated Hamiltonian, the topological invariants for non-Hermitian Hamiltonians, and for more experimental data and its analysis.

[62] M. L. Goldman, M. W. Doherty, A. Sipahigil, N. Y. Yao, S. D. Bennett, N. B. Manson, A. Kubanek, and M. D. Lukin, State-selective intersystem crossing in nitrogen-vacancy centers, Phys. Rev. B **91**, 165201 (2015).

[63] L. Robledo, L. Childress, H. Bernien, B. Hensen, P. F. Alkemade, and R. Hanson, High-fidelity projective read-out of a solid-state spin quantum register, Nature (London) **477**, 574 (2011).

[64] V. Jacques, P. Neumann, J. Beck, M. Markham, D. Twitchen, J. Meijer, F. Kaiser, G. Balasubramanian, F. Jelezko, and J. Wrachtrup, Dynamic Polarization of Single Nuclear Spins by Optical Pumping of Nitrogen-Vacancy Color Centers in Diamond at Room Temperature, Phys. Rev. Lett. **102**, 057403 (2009).

[65] B. Smeltzer, J. McIntyre, and L. Childress, Robust control of individual nuclear spins in diamond, Phys. Rev. A **80**, 050302(R) (2009).

[66] C. Zu, W.-B. Wang, L. He, W.-G. Zhang, C.-Y. Dai, F. Wang, and L.-M. Duan, Experimental realization of universal geometric quantum gates with solid-state spins, Nature (London) **514**, 72 (2014).

[67] T. Van der Sar, Z. Wang, M. Blok, H. Bernien, T. Taminiau, D. Toyli, D. Lidar, D. Awschalom, R. Hanson, and V. Dobrovitski, Decoherence-protected quantum gates for a hybrid solid-state spin register, Nature (London) **484**, 82 (2012).

[68] M. Hayashi, *Asymptotic Theory of Quantum Statistical Inference: Selected Papers* (World Scientific, Singapore, 2005).

[69] T. Fukui, Y. Hatsugai, and H. Suzuki, Chern numbers in discretized brillouin zone: Efficient method of computing (spin) Hall conductances, J. Phys. Soc. Jpn. **74**, 1674 (2005).

[70] N. Okuma, K. Kawabata, K. Shiozaki, and M. Sato, Topological Origin of Non-Hermitian Skin Effects, Phys. Rev. Lett. **124**, 086801 (2020).

[71] K. Zhang, Z. Yang, and C. Fang, Correspondence between Winding Numbers and Skin Modes in Non-Hermitian Systems, Phys. Rev. Lett. **125**, 126402 (2020).